

MEASUREMENTS AND CALCULATIONS ON THE 50-MEV BROOKHAVEN LINAC[†]

K. Batchelor,[‡] R. Chasman and T. Werntz
 Brookhaven National Laboratory
 Upton, L.I., New York

Introduction

The proposed AGS Conversion Program calls for accelerated peak beam currents in excess of 100 mA from the new injector linac. The data presented represent a series of measurements and calculations carried out on the existing linac. Although the results were taken with an accelerated beam current in the region of 30 mA, many of the results are directly applicable to the new proposal since the present cavity length is more than one and a half times greater than any cavity in the new proposal.¹ Measurements of the transient and steady-state phase and amplitude changes between center and end of the center-fed cavity are presented, together with calculated values obtained from the theory of T. Nishikawa.^{2,3} Beam energy measurements are also presented together with some computational data from Brookhaven and from D. Young at MURA.

Computations

Phase and Amplitude Effects

The normal mode analysis developed by T. Nishikawa describes the field distributions inside a long cavity in terms of the fields set up in TM_{01n} modes. In the analysis used here, only excitation of the TM₀₁₀, TM₀₁₁, and TM₀₁₂ modes has been considered, the assumption being that any higher order modes will have only a negligibly small effect on the results. For the AGS linac the frequency differences between the TM₀₁₀ excitation mode frequency and the TM₀₁₁ and TM₀₁₂ mode frequencies were 30 kc/sec and 122 kc/sec, respectively. The cavity is fed at the geometric center but due to drift tube loading effects this does not correspond to the electrical center so there is some excitation of the TM₀₁₁ mode. An estimation of the coupling factor for this mode has been made from observations of the amplitude of the "scallop" that result from excitation of the TM₀₁₁ mode only at ~ L/4 and 3L/4 points, and the TM₀₁₂ mode only at the L/2 point in the cavity. With knowledge of these difference frequencies and the TM₀₁₁ coupling coefficient, the field theory gives values for the transient and steady-state phase and amplitude changes affected by the main excitation pulse. When the beam is introduced into the cavity a further rf pulse is applied in order to compensate for the resistive loss in the beam itself. This compensation pulse

gives rise to further phase and amplitude changes which are of a transient nature due to the short beam pulse length (~ 40 μsec). These phase and amplitude changes occur whether the beam is present or not and the exact values depend upon the shape and timing of the compensation pulse with respect to the beam pulse. The results of these computations are presented with the experimental data for comparison.

Output Energy Spectra

The calculated energy distribution at 50 MeV was obtained by use of a computer program by S. Ohnuma and calculated at Yale. In this program it is assumed that acceleration takes place in an infinitesimally small interval. The transit time factor in each cell is a function of the energy of each individual particle and a change in phase is introduced at the acceleration gap to guarantee conservation of longitudinal phase-space area (Promé approximation). The output energy spectrum was computed for particles with axial displacements up to 7 mm and zero slopes. Such a beam can be obtained by the use of a narrow rectangular slit. It was assumed that the particles were evenly distributed with respect to input phase (corresponding to no buncher) and all had the design input energy. A flat field and a field with 5% tilt with respect to the cavity center, the input end being 10% lower than the output end field level, were considered. In both cases calculations were done for seven different rf levels or synchronous phases. Figures 1 and 2 show the results. The sensitivity of the output energy spread to the rf level can easily be understood if one derives the output phase from the linear theory for axial particles in linear accelerators:

$$\varphi_{\text{output}} = \varphi_{\text{input}} + \int_{\text{output}}^{\text{input}} k_{\ell} ds .$$

Here k_{ℓ} is the longitudinal oscillation wave number and is given by

$$k_{\ell} = \left(\frac{2\pi e E_0 T \sin |\varphi_s|}{mc^2 \beta^3 \gamma^3 \lambda} \right)^{\frac{1}{2}} ,$$

where E_0 = the average electric field gradient,
 T = transit time factor for the synchronous particle,
 φ_s = synchronous phase,
 λ = wavelength of the rf field.

Assuming constant acceleration (flat field and average constant transit time factor) one gets the following results:

[†] Work performed under the auspices of the U.S. Atomic Energy Commission.

[‡] On leave from the Rutherford High Energy Laboratory.

φ_s	Rf Field Level	$\frac{\varphi_{\text{output}} - \varphi_{\text{input}}}{\pi}$
-19°	712	7.15
-20°	716	7.34
-21°	720	7.54
-22°	725	7.74
-23°	731	7.94
-24°	736	8.13
-25°	743	8.31

According to the above figures a change from 24° to 19° in synchronous phase or a change of 3% in rf level will change the output phase by 180°. A change of 1.5% in rf level will therefore be enough to go from minimum to maximum output energy spread.

Experimental Methods

Phase and Amplitude Measurements

A four-arm coaxial line 3 dB hybrid together with a precision calibrated line lengthener were used for the phase measurements. Two long calibrated cables were used to connect to any of a number of accurately made pickup loops situated at intervals along the linac cavity. Small phase shifts were measured by photographing the response of the combined detected output signals from the hybrid and measuring up the photograph for comparison with a calibration curve obtained by varying the phase in one input arm of the bridge by means of the calibrated line stretcher. Larger phase shifts were measured by recording the line length change required to restore the error signal to zero at various points along the error pulse. The system was initially set to a null by connecting the cables to two pickup loops situated very close to each other near the center of the cavity. Measurements were made between the center section and each of the other ten sections which make up the linac cavity.

Amplitude changes were measured by observations on the residual 5% of the detected rf pulse from each of the eleven sections after biasing back with a steady dc voltage. Since changes in coupling loop dimensions affect the results, the accuracies claimed are within 0.5° for phase measurements and ± 0.2% for amplitude measurements. The experimental arrangement is shown in schematic form in Fig. 3.

Beam Energy Observations

During normal operation of the AGS linac, 1 in 3 of the accelerated beam pulses is diverted by means of a 5° bending magnet into a separate beam tube for momentum analysis. This system of

analysis was used for the beam energy observations and is shown in schematic form in Fig. 4.

In order to produce a well-collimated beam to more closely simulate computational methods the preinjector beam was reduced by use of a ½ in. diameter hole followed by a 0.050 in. wide vertical slit ~ 1 ft before the tank and ~ 5 ft beyond the ½ in. hole. The buncher was disconnected and the beam compensation pulse was set to zero since only very low beam currents, ~ 2 mA, were accelerated. The Beam Analysis System comprises a 0.100 in. wide slit collimator, a bending magnet, and a series of 12 slits each 0.030 in. wide and spaced by 0.124 in. behind each of which is situated a Faraday cup. The amplified signals from the Faraday cups are displayed sequentially on an oscilloscope to give the output spectrum, while the bending magnet current is accurately monitored by measuring the voltage across a fixed stable resistor and displaying this voltage digitally. Each cup represents a sample from an integrated 68 keV energy slice of the output beam so any fine structure in the output spectrum is not seen.

Results

Phase and Amplitude Effects

The beam pulse length was 40 usec and the rf pulse length 200 usec so the "steady-state" measurements were taken ~ 150 usec after the rf pulse was switched on. For all measurements with the beam the 50-MeV accelerated peak current was 32 mA. The beam compensation pulse was found to have a rise time of ~ 15 μsec. The steady-state amplitude and phase difference between the center section and each of the other ten sections of the linac was measured with and without the beam present.

The two sets of experimental results for phase shift are plotted as Fig. 5, which also shows the computed curve. The two sets of data should be the same so this gives a measure of the experimental accuracy. It can be seen that agreement between theory and experiment is good at the low energy end and fairly good at the high energy end of the linac. The amplitude variation due to the 32 mA beam loading with a compensation pulse whose amplitude was 10% of the main rf excitation pulse are plotted in Fig. 6. This again shows good agreement between theory and experiment.

The extra phase shift due to a 6% compensation pulse was measured with and without the beam present and the results are plotted in Fig. 7. It can be seen that the results are similar for both cases within the accuracy of the measurement. This is expected since the beam does not couple strongly with the higher order modes which give rise to the phase shifts measured. The transient phase shift due to the main excitation pulse was measured at the input and output ends of the linac and plotted in Figures 8 and 9. Comparison between theory and measurement is again good at the low energy end and fair at the high energy end of the linac.

The detailed amplitude and phase variations at both ends of the cavity during the beam period due to a 6% compensation pulse are shown in Figures 10 and 11. These results clearly show the beat frequencies between the TM_{010} and TM_{011} and TM_{012} modes, respectively.

Energy Spectra

With the collimated beam described earlier the energy spectrum was measured for various rf field levels in the linac. For the first set of measurements the field was that which had been set up by reference to the readings from accurately made pickup loops situated along the length of the cavity. This resulted in an almost flat field along the length of the cavity with the input end field only about 12% higher than the output end. The resulting spectra for various rf field levels are shown in Fig. 12. The movement of the peak of the spectra with increasing rf field level follows the usual pattern observed in the Rutherford High Energy Laboratory proton linac⁴ and is due to the change in phase oscillation wavelength with amplitude as described in the computational section of this report.

D. Young of MURA has computed transit time factors for the Argonne linac and also has experimental data⁵ which suggest that the field gradient in the early gaps should be increased to give "ideal" acceleration. He also modified these results to give the correct law for the BNL linac and this is plotted in Fig. 13. A preliminary attempt was made to set up this field law on the BNL linac but it was found that in order to increase the field gradient sufficiently in the early gaps extra ball tuners would be required. However, the field was increased by about 3% in the early gaps (see Fig. 13) and the spectra for various rf field levels are plotted in Fig. 14.

The spectra were all recorded at very low beam level so that beam loading effects were negligible. When a beam current of 30 mA or more is accelerated the resultant energy spectrum is effectively a summation of a number of the observed spectra since the average rf field amplitude changes by ~ 1.5% during the beam pulse. This, together with coupling between radial and phase motion, results in a wider energy spectrum.

Conclusion

The computational data for phase and amplitude effects in the linac show good agreement with the practical measurements. Deviations from exact agreement may be due to a number of reasons. The axial electric field is not uniform as assumed in the theory and the cavity is not fed from a "matched" source. The beam loading is not uniform along the length of the cavity since much of the injected beam is lost in the early gaps. The estimate of the coupling coefficient for the TM_{011} mode is very approximate due to the difficulty in making the necessary measurements to determine its value.

Qualitatively the energy spectra show good agreement with theory but a more detailed study of

the exact fields in the cavity by means of the perturbation method is necessary before any real quantitative comparison may be made.

Acknowledgements

The authors wish to thank the many people who cooperated with them in making the above measurements; R.B. McKenzie-Wilson and R. Damm for their work on the mechanical equipment, A. Otis and A. van Steenberg for helpful discussions on the beam energy analyzer, and V. Racaniello and the linac operators for their help in running the machine.

References

1. "Alternating-Gradient Synchrotron Conversion Program - Scope of Phase I," BNL 9500, September 1965.
2. T. Nishikawa, "Normal Mode Analysis of Standing Wave Linacs - Field Excitation and Beam Loading in Linac Cavities," BNL Accelerator Dept. Internal Report AADD-87 (1965).
3. T. Nishikawa, "An Approach to the Study of Beam Loading for the Linear Accelerator," Minutes of 1964 Conference on Proton Linear Accelerators, p. 214, MURA 714 (1964).
4. K. Batchelor, "Beam Observations in the P.L.A.," Minutes of Conference on Linear Accelerators for High Energies, p. 235, BNL 6511 (1962).
5. D.E. Young, "Rf Perturbation Measurements in Long Linac Cavities," Proc. 1966 Linear Accelerator Conference, Los Alamos Scientific Laboratory, p. 140.

DISCUSSION

K. BATCHELOR, RHEL

LAPOSTOLLE, CERN: I would just like to ask whether, in the measurements of the energy spectrum at the output, some measurements have been made at different times in the pulse?

BATCHELOR: No, we do not at the moment have the facility to make measurements at various intervals during the pulse. Let me say, that the measurements are made in a sense under extreme difficulty, because there is an absolute jitter on the rf signal in the BNL linac at the moment which, in the worst case, can be in the region of 5%. In order to make these measurements, therefore, we have to display at the same time the rf pulse amplitude and the energy spectrum and photograph the two traces simultaneously. We do have a program which will ultimately close an amplitude control loop on the modulator for the AGS linac, and when this is in operation, further improved measurements will be made. I might add, that the spectrum that one observes during normal operation of the machine is essentially a summation of some of these measured spectra. In fact, I have computed from these spectra a composite spectrum, and this agrees very well with the measured spectrum observed at the measured rf amplitude.

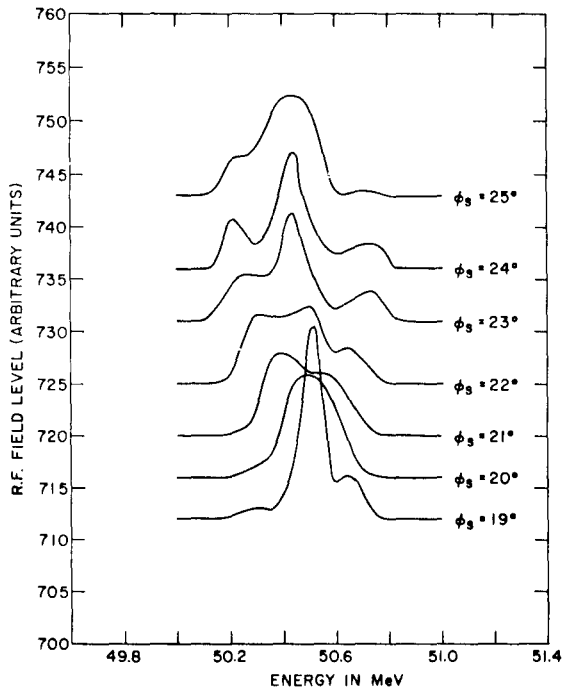


Fig. 1. Computed spectra with "design" field low.

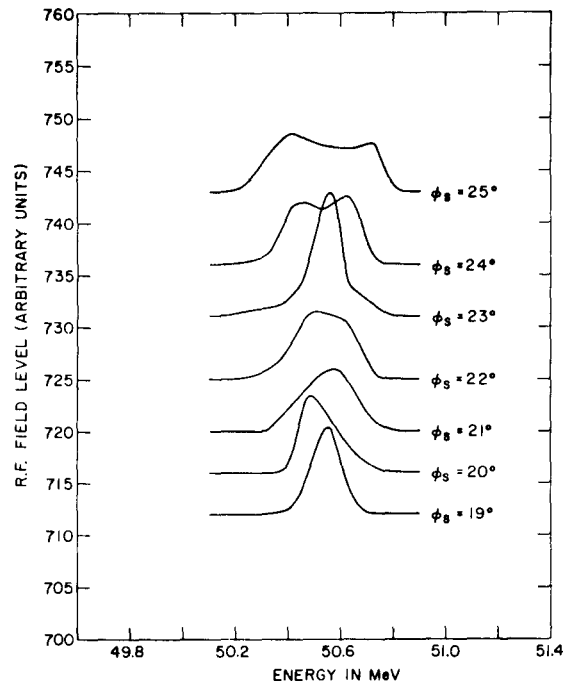


Fig. 2. Computed spectra with 5% tilt on field.

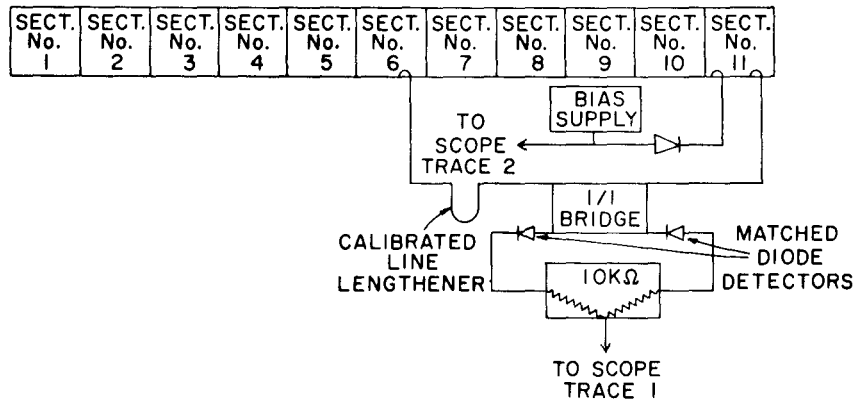


Fig. 3. Experimental arrangement for phase and amplitude measurements.

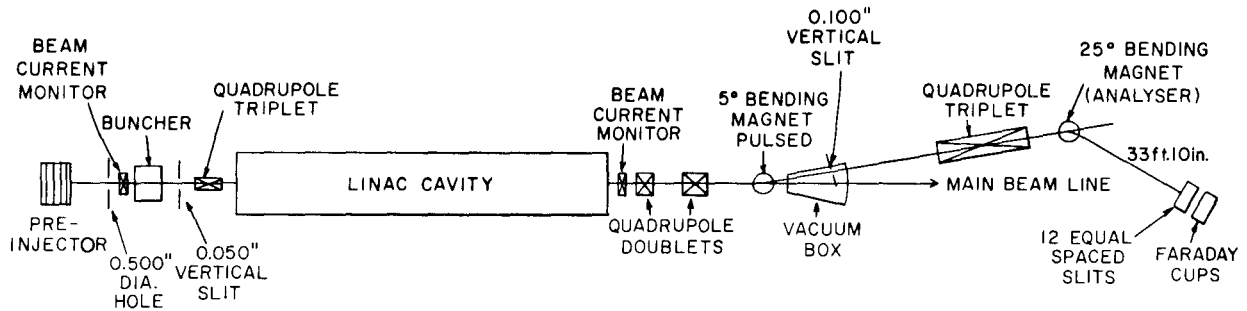


Fig. 4. Experimental arrangement for beam energy measurements.

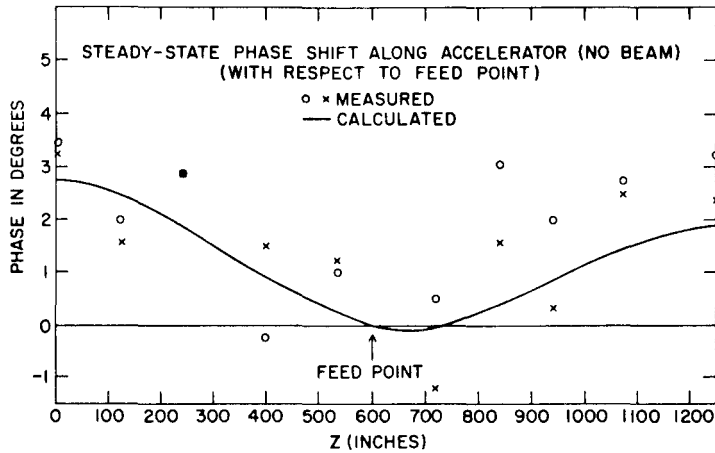


Fig. 5. Steady-state phase shift along accelerator (no beam) with respect to feed points.

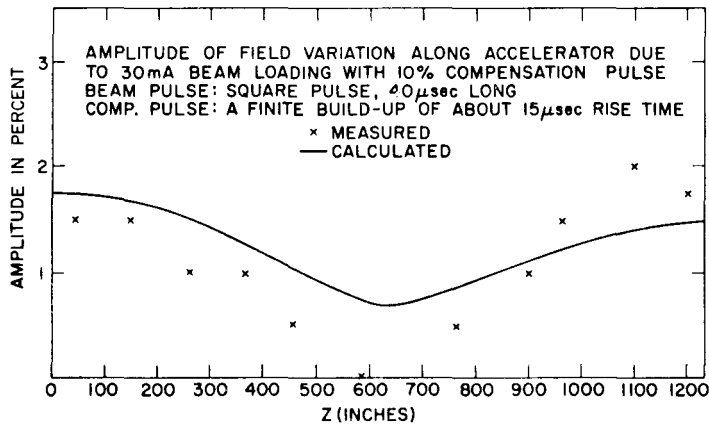


Fig. 6. Amplitude of field variation along accelerator due to 30 mA beam loading with 10% compensation pulse.

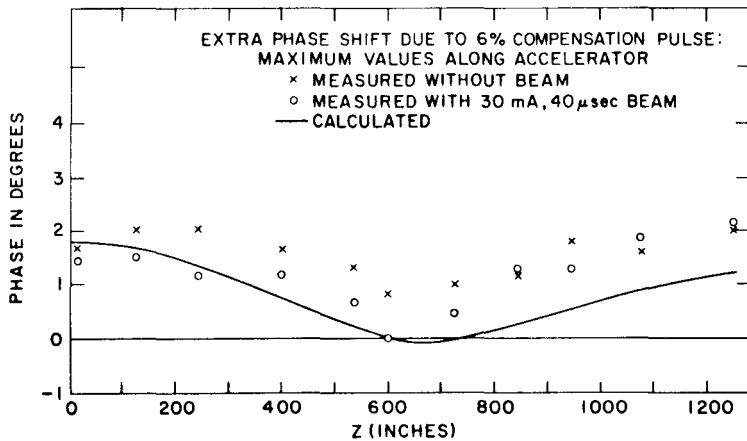


Fig. 7. Extra phase shift due to 6% compensation pulse, maximum values along accelerator.

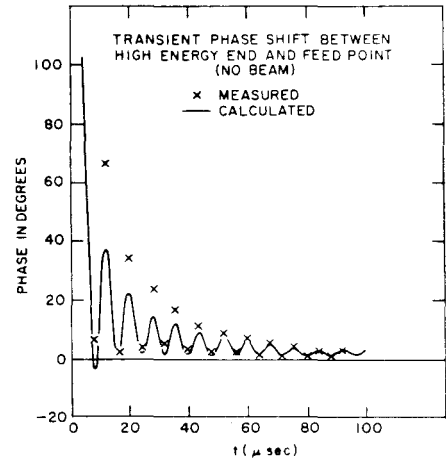


Fig. 8. Transient phase shift between low energy end and feed point (no beam).

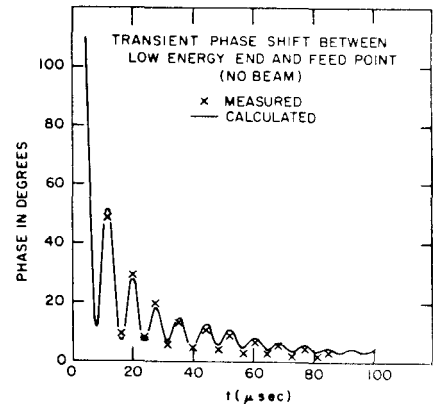


Fig. 9. Transient phase shift between high energy end and feed point (no beam).

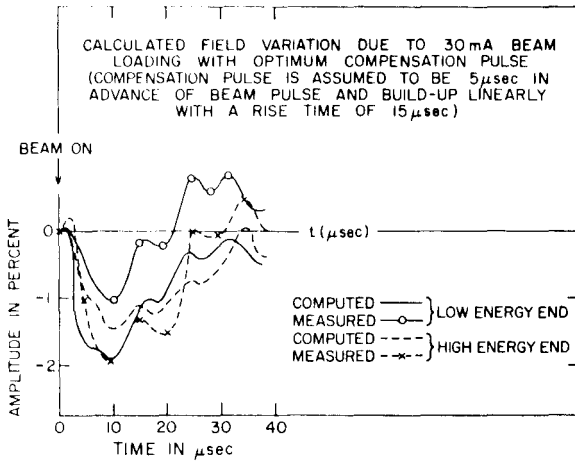


Fig. 10. Calculated field variation due to 30 mA beam loading with optimum compensation pulse.

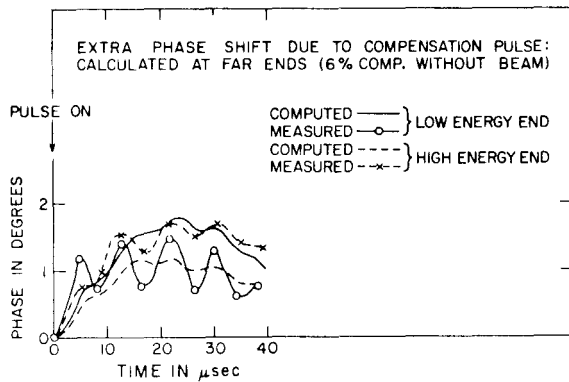


Fig. 11. Extra phase shift due to compensation pulse calculated at far ends (6% compensation without beam).

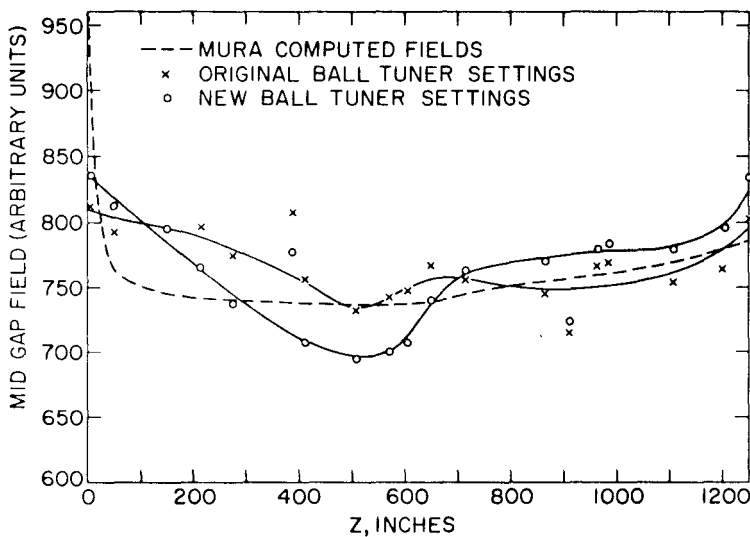


Fig. 13. Cavity axial field gradient (determined from readings on magnetic pick-up probes coupled at the cavity wall).

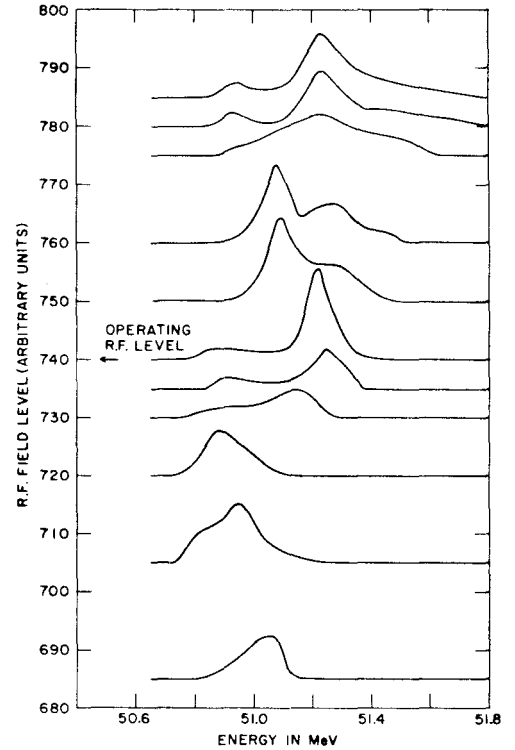


Fig. 12. Measured energy spectra for various rf field levels; ball tuners at original settings.

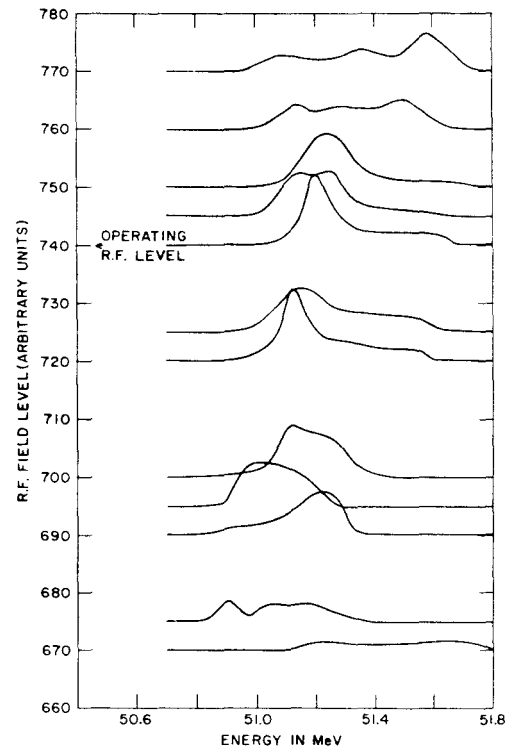


Fig. 14. Measured energy spectra for various rf field levels; new ball tuner settings.